

An Enhanced-Coupling Control Method for Aerial Transportation Systems With Double-Pendulum Swing Effects

Kexin Cai^{ID}, Hai Yu^{ID}, Graduate Student Member, IEEE, Wei He^{ID}, Xiao Liang^{ID}, Member, IEEE, Jianda Han^{ID}, Member, IEEE, and Yongchun Fang^{ID}, Senior Member, IEEE

Abstract—Quadrupedal robots, with significant advantages in flexibility and maneuverability, become an excellent platform for reconnaissance and rescue tasks. When performing cargo delivery tasks, the rotation of the hook around the suspension point, together with the rotation of the cargo around the hook, causes the double-pendulum swing effects. Nevertheless, the underactuated characteristic of the quadrupedal robot and the indirectly controllable motion of the hook and the suspended cargo make the controller design extremely difficult. In this article, considering the double-pendulum effect, an enhanced-coupling control scheme is proposed for aerial transportation systems to achieve better quadrupedal robot positioning, as well as hook and cargo swing elimination. Specifically, an ingenious energy function is constructed by integrating the information of the quadrupedal robot translational motion and double-pendulum swing dynamics, which improves the transient performance of the controller. Compared with existing methods, this article provides the first enhanced-coupling controller design with consideration of both quadrupedal robot and hook/cargo dynamics. Finally, based on the Lyapunov method, the equilibrium point of the closed-loop system is proved asymptotically stable, and several groups of hardware experiments are conducted to validate the feasibility and robustness of the proposed control scheme.

Index Terms—Double-pendulum swing characteristic, energy-based analysis method, enhanced-coupling control method.

Manuscript received 19 October 2022; revised 2 April 2023 and 15 June 2023; accepted 12 September 2023. Date of publication 2 October 2023; date of current version 18 June 2024. Recommended by Technical Editor S. G. Loizou and Senior Editor N. G. Tsagarakis. This work was supported in part by the National Natural Science Foundation of China under Grant 62273187, Grant 62233011, and Grant 91848203, in part by the Young Elite Scientists Sponsorship Program by Tianjin under Grant TJSQNTJ-2020-21, and in part by the Haihe Lab of ITAI under Grant 22HXCJC00003. (Hai Yu is co-first author.) (Corresponding author: Xiao Liang.)

The authors are with the Institute of Robotics and Automatic Information System, College of Artificial Intelligence, and Tianjin Key Laboratory of Intelligent Robotics, Nankai University, Tianjin 300350, China, and also with the Engineering Research Center of Trusted Behavior Intelligence, Ministry of Education, Nankai University, Tianjin 300350, China (e-mail: ckexin@mail.nankai.edu.cn; yuhai@mail.nankai.edu.cn; howei@mail.nankai.edu.cn; liangx@mail.nankai.edu.cn; hanjianda@nankai.edu.cn; fangyc@nankai.edu.cn).

This article has supplementary material provided by the authors and color versions of one or more figures available at <https://doi.org/10.1109/TMECH.2023.3316423>.

Digital Object Identifier 10.1109/TMECH.2023.3316423

I. INTRODUCTION

QUADRUPEDAL unmanned aerial vehicles (UAVs) have demonstrated superior ability in civil applications, such as environmental protection, localization, and delivery of cargos. Because of its excellent properties of maneuverability and flexibility [1], [2], [3], [4], [5], [6], quadrupedal robots are widely utilized in cargo delivery tasks. At present, flying grippers [7], [8], [9], aerial manipulators [10], [11], [12], and slung load systems [13], [14], [15] are typical ways of cargo transportation with quadrupedal robots. Manipulators as well as grippers are able to execute accurate operations for objects with small volume. While cable-suspended payload transportation enjoys the advantage of high agility because of the flexible linkage between the cargo and the quadrupedal robot, resulting in energy efficiency. Moreover, cable-suspended transportation presents a concise mechanical structure because there is no need to consider the design of the manipulator and the gripper.

Classical research works on aerial transportation systems mainly focus on the single-pendulum swing characteristic, which is based on the assumption that the suspension point is close to the center of mass of the aerial vehicle. The aerial transportation system is underactuated because the number of degrees of freedom of the system is greater than its independent inputs [16], [17], [18], [19]. Considering the underactuated property, complex dynamic coupling, and strong nonlinear feature of the system, it is a great challenge to control it with high precision. For such systems, a trajectory tracking controller based on an input-output feedback linearization technology applied to Furuta pendulum was proposed in [16]. In [17], an adaptive neural network-based solution for arm tracking control and pendulum regulation of the Furuta pendulum was given. Wu et al. [18] devised a continuous global sliding mode method for the overhead crane system, in which a nonlinear disturbance observer is utilized for the regulation and disturbance estimation control. In [19], a nonlinear positioning control method was presented to resist unknown environmental disturbances via the adaptive heading assignment for underactuated marine surface vehicles.

In addition to the above underactuated systems, there are many research works on the aerial transportation systems in recent years. Nicotra et al. [20] introduced the nested saturation

control approach, and the asymptotic stability of the aerial vehicle was guaranteed. In [21], an adaptive scheme was designed for a quadrotor that delivers an unknown mass payload by a flexible cable, in which retrospective cost adaptive control is constructed to compensate for the payload mass uncertainty in the case of aggressive maneuvers. A geometric nonlinear control method was adopted in [22] for quadrotor positioning and cargo swing elimination, where the flexible cable is modeled as a system of serially connected links and has been considered in the full dynamic model. A nonlinear hierarchical control method was proposed in [23], which separates the design of the inner loop and the outer loop controller so as to simplify the design process. In [24], a nonlinear backstepping controller was designed for driving the cargo to a predefined trajectory, where Lyapunov and backstepping techniques are used to design the controller. The backstepping technique is allowed to be applied on the cable-suspended cargo-quadrotor system by selecting the backstepping errors carefully, although the cargo translational subsystem and the cargo direction subsystem are in nonstrict feedback form. In [14], a translational control method based on an uncertainty and disturbance estimator was adopted for the design of the outer loop, and an attitude tracking controller was utilized to control the direction of the lift vector. Recently, Muthusamy et al. [25] proposed a nonmodel-based bidirectional fuzzy brain emotional learning controller to handle the cargo uncertainties and disturbances in real time, where a simplified fuzzy neural network structure and a novel bidirectional brain emotional learning algorithm are adopted. In [26], a framework was designed to efficiently generate aggressive load-swing trajectories, where the constraints are embedded into trajectory generation by imposing acceleration limitations on the load. A smooth dynamic feedback method was proposed in [27] for a large class of embedded curves, which guarantees that the cargo converges to the given path and attains path invariance.

By summarizing the above works, it can be seen that most of existing works are based on the simplified single-pendulum model, which ignores the motion of the hook and cannot precisely describe the relative motion between the hook and the cargo in the actual transportation procedure, that is, the double-pendulum swing effect caused by the hook's rotation around the suspension point and the cargo's rotation around the hook are not reflected in dynamics description. While accurately describing the system dynamics, the double-pendulum model exhibits a higher number of degree of freedoms and a more complex dynamic coupling relationship between quadrotor translation and hook/cargo motion.

In the previous work [28], the double-pendulum model in a 3-D space is presented and analyzed for the first time, and a basic nonlinear controller is designed to achieve the desired goal. In this article, an enhanced-coupling feedback controller is proposed to simultaneously suppress swing effects of the cargo and the hook more efficiently. Specifically, an ingenious energy function is constructed by analyzing the system's motion energy and integrating the information of the quadrotor translation and the double-pendulum swing dynamics. Subsequently, a nonlinear controller is designed based on the newly constructed energy storage function. Finally, the asymptotic stability of the proposed

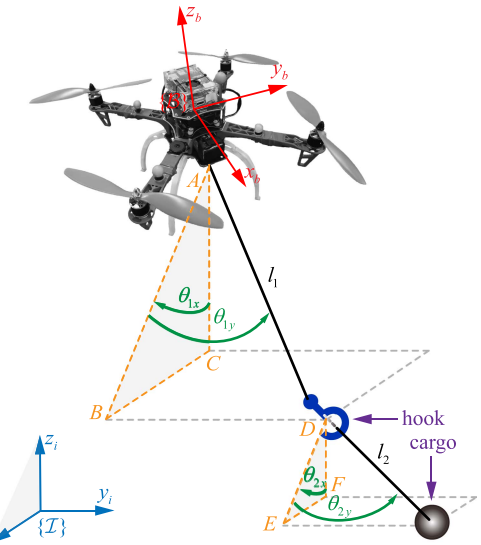


Fig. 1. Schematic diagram of the aerial transportation system with double-pendulum swing dynamics.

control method is proven via Lyapunov-based stability analysis, and hardware experimental results are presented to validate the controller's performance and robustness. The main contributions of this article are summarized as follows:

- 1) By introducing the elaborately constructed real-time swing angle information of cargo and hook into the original error signal, the information of the quadrotor motion and double-pendulum swing dynamics is integrated into the new energy storage function, which can greatly improve the transient control performance in swing suppression.
- 2) Without model linearization or other simplification operations, an effective control scheme is proposed, and the designed controller is in a concise form. In addition, a strict stability proof is provided based on Lyapunov techniques.

The rest of this article is organized as follows. In Section II, the dynamic model and the control problem are provided. Section III presents the enhanced-coupling controller design process. Then, Lyapunov-based stability analysis is provided in Section IV. Hardware experimental tests including performance verification tests and wind disturbance tests are conducted in Section V to verify the performance and robustness of the controller. Finally, Section VI concludes this article.

II. PROBLEM FORMULATION

The schematic diagram of the unmanned aerial transportation system with double-pendulum swing effects is shown in Fig. 1, where $\mathcal{B} = \{x_b, y_b, z_b\}$ and $\mathcal{I} = \{x_i, y_i, z_i\}$ denote the body-fixed frame and the inertial frame, respectively. The dynamic equations are described as follows:

$$(m_0 + m_1 + m_2) \ddot{x} + (m_1 + m_2) l_1 \left(\ddot{\theta}_{1x} C_{1x} C_{1y} - \ddot{\theta}_{1y} \right)$$

$$\begin{aligned} & S_{1x}S_{1y} - \dot{\theta}_{1x}^2 S_{1x}C_{1y} - \dot{\theta}_{1y}^2 S_{1x}C_{1y} - 2\dot{\theta}_{1x}\dot{\theta}_{1y}C_{1x}S_{1y} \\ & + m_2l_2 \left(\ddot{\theta}_{2x}C_{2x}C_{2y} - \ddot{\theta}_{2y}S_{2x}S_{2y} - \dot{\theta}_{2x}^2 S_{2x}C_{2y} - \dot{\theta}_{2y}^2 S_{2x}C_{2y} \right. \\ & \left. - 2\dot{\theta}_{2x}\dot{\theta}_{2y}C_{2x}S_{2y} \right) = f_{s1} \end{aligned} \quad (1)$$

$$\begin{aligned} & (m_0 + m_1 + m_2)\ddot{y} + (m_1 + m_2)l_1 \left(\ddot{\theta}_{1y}C_{1y} - \dot{\theta}_{1y}^2 S_{1y} \right) \\ & + m_2l_2 \left(\ddot{\theta}_{2y}C_{2y} - \dot{\theta}_{2y}^2 S_{2y} \right) = f_{s2} \end{aligned} \quad (2)$$

$$\begin{aligned} & (m_0 + m_1 + m_2)\ddot{z} + (m_1 + m_2)l_1 \left(\ddot{\theta}_{1x}S_{1x}C_{1y} + \dot{\theta}_{1y} \cdot \right. \\ & C_{1x}S_{1y} + \dot{\theta}_{1x}^2 C_{1x}C_{1y} + \dot{\theta}_{1y}^2 C_{1x}C_{1y} - 2\dot{\theta}_{1x}\dot{\theta}_{1y}S_{1x}S_{1y} \\ & \left. + m_2l_2 \left(\ddot{\theta}_{2x}S_{2x}C_{2y} + \ddot{\theta}_{2y}C_{2x}S_{2y} + \dot{\theta}_{2x}^2 C_{2x}C_{2y} + \dot{\theta}_{2y}^2 C_{2x}C_{2y} \right. \right. \\ & \left. \left. - 2\dot{\theta}_{2x}\dot{\theta}_{2y}S_{2x}S_{2y} \right) \right) = f_{s3} - (m_0 + m_1 + m_2)g \end{aligned} \quad (3)$$

$$\begin{aligned} & (m_1 + m_2)l_1C_{1y}(\ddot{x}C_{1x} + \ddot{z}S_{1x}) + (m_1 + m_2)l_1^2C_{1y} \left(\ddot{\theta}_{1x} \cdot \right. \\ & C_{1y} - 2\dot{\theta}_{1x}\dot{\theta}_{1y}S_{1y} \left. \right) + m_2l_1l_2C_{1y} \left(\ddot{\theta}_{2x}C_{2y}C_{(1-2)x} + \ddot{\theta}_{2y} \cdot \right. \\ & S_{2y}S_{(1-2)x} + \dot{\theta}_{2x}^2 C_{2y}S_{(1-2)x} + \dot{\theta}_{2y}^2 C_{2y}S_{(1-2)x} - 2\dot{\theta}_{2x}\dot{\theta}_{2y} \cdot \\ & \left. S_{2y}C_{(1-2)x} \right) + (m_1 + m_2)gl_1S_{1x}C_{1y} = 0 \end{aligned} \quad (4)$$

$$\begin{aligned} & (m_1 + m_2)l_1(-\ddot{x}S_{1x}S_{1y} + \ddot{y}C_{1y} + \ddot{z}C_{1x}S_{1y}) + (m_1 + m_2) \cdot \\ & l_1^2 \left(\dot{\theta}_{1y} + \dot{\theta}_{1x}^2 C_{1y}S_{1y} \right) + m_2l_1l_2 \left[-\ddot{\theta}_{2x}S_{1y}C_{2y}S_{(1-2)x} + \ddot{\theta}_{2y} \cdot \right. \\ & \left. (S_{1y}S_{2y}C_{(1-2)x} + C_{1y}C_{2y}) + \dot{\theta}_{2x}^2 S_{1y}C_{2y}C_{(1-2)x} + \dot{\theta}_{2y}^2 \cdot \right. \\ & \left. (S_{1y}C_{2y}C_{(1-2)x} - C_{1y}S_{2y}) + 2\dot{\theta}_{2x}\dot{\theta}_{2y}S_{1y}S_{2y}S_{(1-2)x} \right] \\ & + (m_1 + m_2)gl_1C_{1x}S_{1y} = 0 \end{aligned} \quad (5)$$

$$\begin{aligned} & m_2l_2C_{2y}(\ddot{x}C_{2x} + \ddot{z}S_{2x}) + m_2l_2^2C_{2y} \left(\ddot{\theta}_{2x}C_{2y} - 2\dot{\theta}_{2x}\dot{\theta}_{2y}S_{2y} \right) \\ & + m_2l_1l_2C_{2y} \left(\dot{\theta}_{1x}C_{1y}C_{(1-2)x} - \dot{\theta}_{1y}S_{1y}S_{(1-2)x} - \dot{\theta}_{1x}^2 \cdot \right. \\ & C_{1y}S_{(1-2)x} - \dot{\theta}_{1y}^2 C_{1y}S_{(1-2)x} - 2\dot{\theta}_{1x}\dot{\theta}_{1y}S_{1y}C_{(1-2)x} \left. \right) \\ & + m_2gl_2S_{2x}C_{2y} = 0 \end{aligned} \quad (6)$$

$$\begin{aligned} & m_2l_2(-\ddot{x}S_{2x}S_{2y} + \ddot{y}C_{2y} + \ddot{z}C_{2x}S_{2y}) + m_2l_2^2 \left(\ddot{\theta}_{2y} + \dot{\theta}_{2x}^2 C_{2y} \cdot \right. \\ & \left. S_{2y} \right) + m_2l_1l_2 \left[\dot{\theta}_{1x}C_{1y}S_{2y}S_{(1-2)x} + \dot{\theta}_{1y} \left(C_{1y}C_{2y} + S_{1y}S_{2y} \cdot \right. \right. \\ & \left. \left. \right. \right] \end{aligned}$$

$$\begin{aligned} & C_{(1-2)x} \right) + \dot{\theta}_{1x}^2 C_{1y}S_{2y}C_{(1-2)x} + \dot{\theta}_{1y}^2 \left(-S_{1y}C_{2y} + C_{1y}S_{2y} \cdot \right. \\ & C_{(1-2)x} \left. \right) - 2\dot{\theta}_{1x}\dot{\theta}_{1y}S_{1y}S_{2y}S_{(1-2)x} \Big] + m_2gl_2C_{2x}S_{2y} = 0 \end{aligned} \quad (7)$$

where m_0, m_1 , and m_2 denote the quadrotor, hook, and cargo masses, respectively. l_1 and l_2 denote the length of the suspension cable and the distance between the hook and the cargo, respectively. g stands for the gravitational constant. $\xi(t) = [x(t), y(t), z(t)]^\top$ denotes the quadrotor position. $\Theta_1(t) = [\theta_{1x}(t), \theta_{1y}(t)]^\top$ and $\Theta_2(t) = [\theta_{2x}(t), \theta_{2y}(t)]^\top$ are the swing angles of the hook and the cargo, respectively. $C_{1x}, S_{1x}, C_{1y}, S_{1y}, C_{2x}, S_{2x}, C_{2y}, S_{2y}, C_{(1-2)x}$, and $S_{(1-2)x}$ are abbreviations of $\cos(\theta_{1x}), \sin(\theta_{1x}), \cos(\theta_{1y}), \sin(\theta_{1y}), \cos(\theta_{2x}), \sin(\theta_{2x}), \cos(\theta_{2y}), \sin(\theta_{2y}), \cos(\theta_{1x} - \theta_{2x})$, and $\sin(\theta_{1x} - \theta_{2x})$, respectively. The auxiliary planes ABC and DEF are labeled in Fig. 1, which are parallel to the $x_i z_i$ plane, lines AC and DF are parallel to the z_i -axis, and lines BC and EF are parallel to the x_i -axis. The auxiliary line segments AB and DE represent the projection of the corresponding suspension cable on the planes ABC and DEF , respectively. Further, θ_{1x} is the angle between AB and AC , and θ_{2x} is the angle between DE and DF . θ_{1y} and θ_{2y} are defined as the angles between the corresponding suspension cable and the auxiliary lines AB and CD , respectively. The positive or negative values of θ_{1x} and θ_{1y} are determined by the vector that points from the suspension point to the hook. Specifically, θ_{1x} is positive when the projection of vector \overrightarrow{AD} is positive on the x_i -axis, and θ_{1y} is positive when the projection of this vector is positive on the y_i -axis. Similarly, the positive or negative values of angles θ_{2x} and θ_{2y} are determined by the vector of the hook pointing to the cargo. $f_s(t) \in \mathbb{R}$ denotes the applied thrust force. $R(t) \in SO(3)$ is the rotation matrix from the body-fixed frame to the inertial frame. f_{s1}, f_{s2} , and f_{s3} stand for the three elements of the vector $f_s R e_3$ with $e_3 = [0, 0, 1]^\top$. For the sake of subsequent analysis, $f_s R e_3$ is divided into the following two parts:

$$\begin{aligned} f_s R e_3 = & \underbrace{\frac{f_s}{e_3^\top R_d^\top R e_3} [(e_3^\top R_d^\top R e_3) R e_3 - R_d e_3]}_{\Delta} \\ & + \underbrace{\frac{f_s}{e_3^\top R_d^\top R e_3} R_d e_3}_f \end{aligned}$$

where $R_d \in SO(3)$ denotes the desired attitude for the inner loop subsystem, $f(t) = [f_x(t), f_y(t), f_z(t)]^\top$ is the to-be-constructed virtual control vector, and $\Delta \in \mathbb{R}^3$ denotes the auxiliary signal, which is the error between the actual force vector $f_s R e_3$ and the virtual control vector f . Neglecting the coupling term Δ temporarily [3], [23], i.e., $\Delta = 0$. Define the state vector $q(t) \in \mathbb{R}^7$ as

$$\begin{aligned} q(t) &= [\xi(t)^\top, \Theta_1(t)^\top, \Theta_2(t)^\top]^\top \\ &= [x(t), y(t), z(t), \theta_{1x}(t), \theta_{1y}(t), \theta_{2x}(t), \theta_{2y}(t)]^\top. \end{aligned}$$

Further, (1)–(7) can be written in a compact form as

$$M(\mathbf{q})\ddot{\mathbf{q}} + V_c(\mathbf{q}, \dot{\mathbf{q}})\dot{\mathbf{q}} + \mathbf{G}(\mathbf{q}) = \mathbf{u} \quad (8)$$

where the form of the inertia matrix $M(\mathbf{q}) \in \mathbb{R}^{7 \times 7}$, the centrifugal-Coriolis matrix $V_c(\mathbf{q}, \dot{\mathbf{q}}) \in \mathbb{R}^{7 \times 7}$, and the gravity vector $\mathbf{G}(\mathbf{q}) \in \mathbb{R}^7$ are provided in the Appendix. The resultant force applied to the outer loop subsystem $\mathbf{u} = [(\mathbf{f} - (m_0 + m_1 + m_2)g\mathbf{e}_3)^\top, 0, 0, 0, 0]^\top$.

Property 1: The centripetal-Coriolis matrix V_c and the time derivative of M satisfy the skew-symmetric relationship [29], i.e., $\chi^\top (\frac{1}{2}\dot{M} - V_c)\chi = 0 \forall \chi \in \mathbb{R}^7$.

As widely satisfied in literatures [20], [23], [30], and [31], the following reasonable assumptions are made.

Assumption 1: Neither the hook nor the cargo will not turn upside down, i.e.

$$-\pi/2 < \theta_{1x}(t), \theta_{1y}(t), \theta_{2x}(t), \theta_{2y}(t) < \pi/2. \quad (9)$$

Assumption 2: The suspension cables connecting the cargo, the hook, and the quadrotor are always taut.

Remark 1: In fact, for such transportation systems as cranes and aerial transportation systems [20], [23], [30], [31], the cable is always rigid, unless the platform or cargo is in unexpected motion. When the suspension cable is slack, the system needs to be remodeled, we will consider modeling the system to be a differentially flat hybrid system with the cargo position and the quadrotor yaw serving as the flat outputs. The modeling method in [32], [33] and the corresponding controller design approach will be referred to cope with the situation that the cable is slack.

This article will provide an effective control scheme aiming at positioning the quadrotor to the desired location and suppressing the double-pendulum swing simultaneously, which could be mathematically described as follows:

$$\begin{aligned} \lim_{t \rightarrow \infty} x(t) &= x_d, \lim_{t \rightarrow \infty} y(t) = y_d, \lim_{t \rightarrow \infty} z(t) = z_d \\ \lim_{t \rightarrow \infty} \theta_{1x}(t) &= 0, \lim_{t \rightarrow \infty} \theta_{1y}(t) = 0 \\ \lim_{t \rightarrow \infty} \theta_{2x}(t) &= 0, \lim_{t \rightarrow \infty} \theta_{2y}(t) = 0 \end{aligned} \quad (10)$$

where $\xi_d = [x_d, y_d, z_d]^\top$ stands for the desired position. To facilitate the controller design, the following error signal is defined:

$$e_\xi(t) = \xi(t) - \xi_d = [e_x(t), e_y(t), e_z(t)]^\top \quad (11)$$

thus, one can obtain that

$$\dot{e}_\xi = \dot{\xi}, \dot{e}_x = \dot{x}, \dot{e}_y = \dot{y}, \dot{e}_z = \dot{z} \quad (12)$$

$$\ddot{e}_\xi = \ddot{\xi}, \ddot{e}_x = \ddot{x}, \ddot{e}_y = \ddot{y}, \ddot{e}_z = \ddot{z} \quad (13)$$

which will be used for the subsequent energy storage function construction and controller development.

III. CONTROLLER DESIGN

In this section, a novel energy storage function is constructed based on a composite signal. Then, the enhanced-coupling controller is designed. The controller design procedure is shown in Fig. 2.

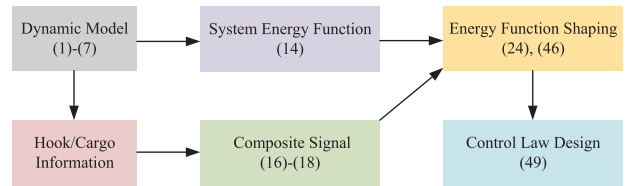


Fig. 2. Flowchart of the controller design procedure.

A. Energy Storage Function Construction

The system energy can be represented in the following way:

$$\begin{aligned} E_o &= \frac{1}{2}\dot{\mathbf{q}}^\top M(\mathbf{q})\dot{\mathbf{q}} + (m_1 + m_2)gl_1(1 - C_{1x}C_{1y}) \\ &\quad + m_2gl_2(1 - C_{2x}C_{2y}). \end{aligned} \quad (14)$$

Based on *Property 1*, differentiating $E_o(t)$ with respect to time and substituting (8) into the resulting equation, it is derived that

$$\begin{aligned} \dot{E}_o &= \dot{\mathbf{q}}^\top \left(M\ddot{\mathbf{q}} + \frac{1}{2}\dot{M}\dot{\mathbf{q}} \right) + (m_1 + m_2)gl_1 \left(\dot{\theta}_{1x}S_{1x}C_{1y} \right. \\ &\quad \left. + \dot{\theta}_{1y}C_{1x}S_{1y} \right) + m_2gl_2 \left(\dot{\theta}_{2x}S_{2x}C_{2y} + \dot{\theta}_{2y}C_{2x}S_{2y} \right) \\ &= \dot{\mathbf{q}}^\top \mathbf{u} - \dot{\mathbf{q}}^\top \mathbf{G} + \frac{1}{2}\dot{\mathbf{q}}^\top \left(\dot{M} - 2V_c \right) \dot{\mathbf{q}} \\ &\quad + (m_1 + m_2)gl_1 \left(\dot{\theta}_{1x}S_{1x}C_{1y} + \dot{\theta}_{1y}C_{1x}S_{1y} \right) \\ &\quad + m_2gl_2 \left(\dot{\theta}_{2x}S_{2x}C_{2y} + \dot{\theta}_{2y}C_{2x}S_{2y} \right) \\ &= \dot{\mathbf{q}}^\top \mathbf{u} = \dot{\xi}^\top [\mathbf{f} - (m_0 + m_1 + m_2)g\mathbf{e}_3] = \dot{\xi}^\top \mathbf{u}_f \end{aligned} \quad (15)$$

where $\mathbf{u}_f = [u_x, u_y, u_z]^\top = \mathbf{f} - (m_0 + m_1 + m_2)g\mathbf{e}_3$. It is worth noting that the second and third terms of (14) reflect the potential energy of the hook and the cargo, and cannot be removed because they are an indispensable part for the controller design and stability analysis.

According to (15), one can see that the system energy $E_o(t)$ is damped out by the actuated quadrotor flight motion $\dot{\xi}(t)$, while the hook and the cargo swing motions are not reflected. To further improve the control performance, an ideal method is to utilize the inherent coupling existing between the actuated quadrotor translation and the unactuated hook/cargo motion. To this end, we will first construct a novel energy storage function based on the introduced composite signal incorporating information of both the quadrotor motion and the double-pendulum swing dynamics.

Considering the dynamics of the quadrotor and the hook/cargo, the following composite signal $\gamma = [\gamma_x, \gamma_y, \gamma_z]^\top$ is introduced as:

$$\gamma_x = x + k_1S_{1x}C_{1y} + k_2S_{2x}C_{2y} \quad (16)$$

$$\gamma_y = y + k_1S_{1y} + k_2S_{2y} \quad (17)$$

$$\gamma_z = z + k_1(1 - C_{1x}C_{1y}) + k_2(1 - C_{2x}C_{2y}) \quad (18)$$

where k_1 and k_2 are control gains to be determined. According to the form of \dot{E}_o in (15), one can elaborately construct \dot{E}_r as

$$\begin{aligned}\dot{E}_r &= \dot{\gamma}^\top \mathbf{u}_f \\ &= \dot{E}_o + k_1 \left[u_x \left(\dot{\theta}_{1x} C_{1x} C_{1y} - \dot{\theta}_{1y} S_{1x} S_{1y} \right) + u_y \dot{\theta}_{1y} C_{1y} \right. \\ &\quad \left. + u_z \left(\dot{\theta}_{1x} S_{1x} C_{1y} + \dot{\theta}_{1y} C_{1x} S_{1y} \right) \right] + k_2 \left[u_x \left(\dot{\theta}_{2x} C_{2x} C_{2y} \right. \right. \\ &\quad \left. \left. - \dot{\theta}_{2y} S_{2x} S_{2y} \right) + u_y \dot{\theta}_{2y} C_{2y} + u_z \left(\dot{\theta}_{2x} S_{2x} C_{2y} \right. \right. \\ &\quad \left. \left. + \dot{\theta}_{2y} C_{2x} S_{2y} \right) \right] \\ &= \dot{E}_o + \dot{E}_{11} + \dot{E}_{12} + \dot{E}_{21} + \dot{E}_{22}\end{aligned}\quad (19)$$

where

$$\dot{E}_{11} = k_1 \dot{\theta}_{1x} (u_x C_{1x} C_{1y} + u_z S_{1x} C_{1y}) \quad (20)$$

$$\dot{E}_{12} = k_1 \dot{\theta}_{1y} (-u_x S_{1x} S_{1y} + u_y C_{1y} + u_z C_{1x} S_{1y}) \quad (21)$$

$$\dot{E}_{21} = k_2 \dot{\theta}_{2x} (u_x C_{2x} C_{2y} + u_z S_{2x} C_{2y}) \quad (22)$$

$$\dot{E}_{22} = k_2 \dot{\theta}_{2y} (-u_x S_{2x} S_{2y} + u_y C_{2y} + u_z C_{2x} S_{2y}). \quad (23)$$

In order to derive a positive definite storage function, $\dot{E}_{11} + \dot{E}_{12} + \dot{E}_{21} + \dot{E}_{22}$ needs to be integrable w.r.t. time. The energy function can be shaped as

$$E_r = E_o + E_a \quad (24)$$

where $E_a = \int_0^t (\dot{E}_{11} + \dot{E}_{12} + \dot{E}_{21} + \dot{E}_{22}) dt$. By substituting (1)–(3) into (20)–(23), \dot{E}_{11} , \dot{E}_{12} , \dot{E}_{21} , and \dot{E}_{22} can be rewritten as

$$\begin{aligned}\dot{E}_{11} &= k_1 \dot{\theta}_{1x} \left[(m_0 + m_1 + m_2) (C_{1x} C_{1y} \ddot{x} + S_{1x} C_{1y} \ddot{z}) + (m_1 \right. \\ &\quad \left. + m_2) l_1 \left(C_{1y}^2 \ddot{\theta}_{1x} - 2C_{1y} S_{1y} \dot{\theta}_{1x} \dot{\theta}_{1y} \right) + m_2 l_2 \lambda_1 \right] \quad (25)\end{aligned}$$

$$\begin{aligned}\dot{E}_{12} &= k_1 \dot{\theta}_{1y} \left[(m_0 + m_1 + m_2) (-S_{1x} S_{1y} \ddot{x} + C_{1y} \ddot{y} + C_{1x} S_{1y} \cdot \right. \\ &\quad \left. \ddot{z}) + (m_1 + m_2) l_1 \left(\ddot{\theta}_{1y} + C_{1y} S_{1y} \dot{\theta}_{1x}^2 \right) + m_2 l_2 \lambda_2 \right] \quad (26)\end{aligned}$$

$$\begin{aligned}\dot{E}_{21} &= k_2 \dot{\theta}_{2x} \left[(m_0 + m_1 + m_2) (C_{2x} C_{2y} \ddot{x} + S_{2x} C_{2y} \ddot{z}) + (m_1 \right. \\ &\quad \left. + m_2) l_1 \lambda_3 + m_2 l_2 (C_{2y}^2 \ddot{\theta}_{2x} - 2C_{2y} S_{2y} \dot{\theta}_{2x} \dot{\theta}_{2y}) \right] \quad (27)\end{aligned}$$

$$\begin{aligned}\dot{E}_{22} &= k_2 \dot{\theta}_{2y} \left[(m_0 + m_1 + m_2) (-S_{2x} S_{2y} \ddot{x} + C_{2y} \ddot{y} + C_{2x} S_{2y} \cdot \right. \\ &\quad \left. \ddot{z}) + (m_1 + m_2) l_1 \lambda_4 + m_2 l_2 (\ddot{\theta}_{2y} + C_{2y} S_{2y} \dot{\theta}_{2x}^2) \right] \quad (28)\end{aligned}$$

where

$$\begin{aligned}\lambda_1 &= C_{(1-2)x} C_{1y} C_{2y} \ddot{\theta}_{2x} + S_{(1-2)x} C_{1y} S_{2y} \ddot{\theta}_{2y} + S_{(1-2)x} \cdot \\ &\quad C_{1y} C_{2y} \dot{\theta}_{2x}^2 + S_{(1-2)x} C_{1y} C_{2y} \dot{\theta}_{2y}^2 - 2C_{(1-2)x} C_{1y} S_{2y} \cdot \\ &\quad \dot{\theta}_{2x} \dot{\theta}_{2y}\end{aligned}$$

$$\begin{aligned}\lambda_2 &= -S_{(1-2)x} S_{1y} C_{2y} \ddot{\theta}_{2x} + (C_{(1-2)x} S_{1y} S_{2y} + C_{1y} C_{2y}) \ddot{\theta}_{2y} \\ &\quad + C_{(1-2)x} S_{1y} C_{2y} \dot{\theta}_{2x}^2 + (C_{(1-2)x} S_{1y} C_{2y} - C_{1y} S_{2y}) \dot{\theta}_{2y}^2\end{aligned}$$

$$\begin{aligned}&+ 2S_{(1-2)x} S_{1y} S_{2y} \dot{\theta}_{2x} \dot{\theta}_{2y} \\ \lambda_3 &= C_{(1-2)x} C_{1y} C_{2y} \ddot{\theta}_{1x} - S_{(1-2)x} S_{1y} C_{2y} \ddot{\theta}_{1y} - S_{(1-2)x} C_{1y} \cdot \\ &\quad C_{2y} \dot{\theta}_{1x}^2 - S_{(1-2)x} C_{1y} C_{2y} \dot{\theta}_{1y}^2 - 2C_{(1-2)x} S_{1y} C_{2y} \dot{\theta}_{1x} \dot{\theta}_{1y} \\ \lambda_4 &= S_{(1-2)x} C_{1y} S_{2y} \ddot{\theta}_{1x} + (C_{(1-2)x} S_{1y} S_{2y} + C_{1y} C_{2y}) \ddot{\theta}_{1y} \\ &\quad + C_{(1-2)x} C_{1y} S_{2y} \dot{\theta}_{1x}^2 + (C_{(1-2)x} C_{1y} S_{2y} - S_{1y} C_{2y}) \dot{\theta}_{1y}^2 \\ &- 2S_{(1-2)x} S_{1y} S_{2y} \dot{\theta}_{1x} \dot{\theta}_{1y}.\end{aligned}$$

Subsequently, inserting (4)–(7) into (25)–(28) and making some arrangements leads to

$$\begin{aligned}\dot{E}_{11} &= -k_1 \dot{\theta}_{1x} \left[m_0 l_1 \left(C_{1y}^2 \ddot{\theta}_{1x} - 2C_{1y} S_{1y} \dot{\theta}_{1x} \dot{\theta}_{1y} \right) + \frac{m_0 m_2 l_2}{m_1 + m_2} \cdot \right. \\ &\quad \left. \lambda_1 + (m_0 + m_1 + m_2) g S_{1x} C_{1y} \right] \quad (29)\end{aligned}$$

$$\begin{aligned}\dot{E}_{12} &= -k_1 \dot{\theta}_{1y} \left[m_0 l_1 \left(\ddot{\theta}_{1y} + C_{1y} S_{1y} \dot{\theta}_{1x}^2 \right) + \frac{m_0 m_2 l_2}{m_1 + m_2} \lambda_2 \right. \\ &\quad \left. + (m_0 + m_1 + m_2) g C_{1x} S_{1y} \right] \quad (30)\end{aligned}$$

$$\begin{aligned}\dot{E}_{21} &= -k_2 \dot{\theta}_{2x} \left[m_0 l_1 \lambda_3 + (m_0 + m_1) l_2 \left(C_{2y}^2 \ddot{\theta}_{2x} - 2C_{2y} S_{2y} \cdot \right. \right. \\ &\quad \left. \left. \dot{\theta}_{2x} \dot{\theta}_{2y} \right) + (m_0 + m_1 + m_2) g S_{2x} C_{2y} \right] \quad (31)\end{aligned}$$

$$\begin{aligned}\dot{E}_{22} &= -k_2 \dot{\theta}_{2y} \left[m_0 l_1 \lambda_4 + (m_0 + m_1) l_2 (\ddot{\theta}_{2y} + C_{2y} S_{2y} \dot{\theta}_{2x}^2) \right. \\ &\quad \left. + (m_0 + m_1 + m_2) g C_{2x} S_{2y} \right]. \quad (32)\end{aligned}$$

Collecting up (29)–(32), the result of \dot{E}_a can be expressed as

$$\dot{E}_a = \dot{E}_{a1} + \dot{E}_{a2} + \dot{E}_{a3} \quad (33)$$

where

$$\begin{aligned}\dot{E}_{a1} &= -(m_0 + m_1 + m_2) g \left(k_1 \dot{\theta}_{1x} S_{1x} C_{1y} + k_1 \dot{\theta}_{1y} C_{1x} S_{1y} \right. \\ &\quad \left. + k_2 \dot{\theta}_{2x} S_{2x} C_{2y} + k_2 \dot{\theta}_{2y} C_{2x} S_{2y} \right) \quad (34)\end{aligned}$$

$$\begin{aligned}\dot{E}_{a2} &= -m_0 l_1 k_1 \left(\dot{\theta}_{1y} \ddot{\theta}_{1y} + C_{1y}^2 \dot{\theta}_{1x} \ddot{\theta}_{1x} - C_{1y} S_{1y} \dot{\theta}_{1x}^2 \dot{\theta}_{1y} \right) - (m_0 \right. \\ &\quad \left. + m_1) l_2 k_2 \left(\dot{\theta}_{2y} \ddot{\theta}_{2y} + C_{2y}^2 \dot{\theta}_{2x} \ddot{\theta}_{2x} - C_{2y} S_{2y} \dot{\theta}_{2x}^2 \dot{\theta}_{2y} \right) \quad (35)\end{aligned}$$

$$\begin{aligned}\dot{E}_{a3} &= -k_1 \frac{m_0 m_2 l_2}{m_1 + m_2} \dot{\theta}_{1x} \lambda_1 - k_1 \frac{m_0 m_2 l_2}{m_1 + m_2} \dot{\theta}_{1y} \lambda_2 \\ &\quad - k_2 m_0 l_1 \dot{\theta}_{2x} \lambda_3 - k_2 m_0 l_1 \dot{\theta}_{2y} \lambda_4. \quad (36)\end{aligned}$$

It can be seen that \dot{E}_{a1} and \dot{E}_{a2} are integrable with respect to time, and one can derive that

$$\begin{aligned}E_{a1} &= -(m_0 + m_1 + m_2) g k_1 (1 - C_{1x} C_{1y}) \\ &\quad - (m_0 + m_1 + m_2) g k_2 (1 - C_{2x} C_{2y}) \quad (37)\end{aligned}$$

$$\begin{aligned}E_{a2} &= -\frac{m_0 l_1}{2} k_1 \left(\dot{\theta}_{1y}^2 + C_{1y}^2 \dot{\theta}_{1x}^2 \right) \\ &\quad - \frac{(m_0 + m_1) l_2}{2} k_2 \left(\dot{\theta}_{2y}^2 + C_{2y}^2 \dot{\theta}_{2x}^2 \right). \quad (38)\end{aligned}$$

To ensure that \dot{E}_{a3} can be integrated versus time, let

$$k_1 \frac{m_0 m_2 l_2}{m_1 + m_2} = k_2 m_0 l_1 \Rightarrow k_2 = \frac{m_2 l_2}{(m_1 + m_2) l_1} k_1. \quad (39)$$

Then, the following conclusion can be yielded:

$$\begin{aligned} E_{a3} = & -m_0 l_1 k_2 \left[C_{(1-2)x} C_{1y} C_{2y} \dot{\theta}_{1x} \dot{\theta}_{2x} + S_{(1-2)x} C_{1y} S_{2y} \cdot \right. \\ & \dot{\theta}_{1x} \dot{\theta}_{2y} - S_{(1-2)y} S_{1y} C_{2y} \dot{\theta}_{1y} \dot{\theta}_{2x} + \left(C_{(1-2)x} S_{1y} S_{2y} \right. \\ & \left. \left. + C_{1y} C_{2y} \right) \dot{\theta}_{1y} \dot{\theta}_{2y} \right]. \end{aligned} \quad (40)$$

By choosing $k_1, k_2 < 0$, it can be proven that E_r is a positive definite scalar function based on the results in (14), (24), (37), (38), and (40), which will be further proved in Section IV.

B. Controller Development

For the composite signal γ in (16)–(18), the control objective in (10) can be equivalently expressed as

$$\begin{aligned} \lim_{t \rightarrow \infty} \gamma_x(t) &= x_d, \lim_{t \rightarrow \infty} \gamma_y(t) = y_d, \lim_{t \rightarrow \infty} \gamma_z(t) = z_d \\ \lim_{t \rightarrow \infty} \theta_{1x}(t) &= 0, \lim_{t \rightarrow \infty} \theta_{1y}(t) = 0 \\ \lim_{t \rightarrow \infty} \theta_{2x}(t) &= 0, \lim_{t \rightarrow \infty} \theta_{2y}(t) = 0 \end{aligned} \quad (41)$$

based on which, the following error signal $e_\gamma(t) = \gamma(t) - \xi_d = [e_{\gamma x}(t), e_{\gamma y}(t), e_{\gamma z}(t)]^\top$ is defined:

$$e_{\gamma x} = \gamma_x - x_d = e_x + k_1 S_{1x} C_{1y} + k_2 S_{2x} C_{2y} \quad (42)$$

$$e_{\gamma y} = \gamma_y - y_d = e_y + k_1 S_{1y} + k_2 S_{2y} \quad (43)$$

$$e_{\gamma z} = \gamma_z - z_d = e_z + k_1 (1 - C_{1x} C_{1y}) + k_2 (1 - C_{2x} C_{2y}) \quad (44)$$

and it is obvious that

$$\dot{e}_\gamma = \dot{\gamma}. \quad (45)$$

In light of (24) and (42)–(44), we elaborately construct the following energy-like nonnegative function so as to inject the newly defined error signals into the system:

$$V = E_r + [k_{px}, k_{py}, k_{pz}] \ln \cosh(e_\gamma) \quad (46)$$

where $k_{px}, k_{py}, k_{pz} \in \mathbb{R}_+$ represent positive control gains, and $\ln \cosh(e_\gamma) = [\ln \cosh(e_{\gamma x}), \ln \cosh(e_{\gamma y}), \ln \cosh(e_{\gamma z})]^\top \in \mathbb{R}^3$. Taking the time derivative of $V(t)$ in (46) and making use of (19), we are led to the following result:

$$\dot{V} = \dot{e}_\gamma^\top [u_f + K_p \tanh(e_\gamma)] \quad (47)$$

where $K_p = \text{diag}([k_{px}, k_{py}, k_{pz}]) \in \mathbb{R}_+^{3 \times 3}$ denotes a diagonal, positive-definite gain matrix, and $\tanh(e_\gamma) = [\tanh(e_{\gamma x}), \tanh(e_{\gamma y}), \tanh(e_{\gamma z})]^\top \in \mathbb{R}^3$. Hence, the enhanced-coupling controller can be designed as follows:

$$u_f = -K_p \tanh(e_\gamma) - K_d \tanh(\dot{e}_\gamma) \quad (48)$$

where $K_d = \text{diag}([k_{dx}, k_{dy}, k_{dz}])$ represents a positive definite, diagonal control matrix. The virtual control vector f for the

system can be written in the following form:

$$f = -K_p \tanh(e_\gamma) - K_d \tanh(\dot{e}_\gamma) + (m_0 + m_1 + m_2) g e_3. \quad (49)$$

In fact, by properly choosing the control parameters, the input amplitude can be kept in a preset scope.

Remark 2: The proposed controller is designed for rigid-body quadrotor, and the thrust force f_s and the three torques $\tau = [\tau_1, \tau_2, \tau_3]^\top \in \mathbb{R}^3$ can be obtained according to the designed virtual control vector f . From $f = \frac{f_s}{e_3^\top R_d^\top R e_3} R_d e_3$, one can find that f and $R_d e_3$ have the same direction, then a desired unit direction vector $r_{3d} = R_d e_3 \in \mathbb{R}^3$ can be obtained by $r_{3d} = R_d e_3 = \frac{f}{\|f\|}$. Thus, f can be further arranged as

$$f = \frac{f_s \|f\|}{f^\top R e_3} \cdot \frac{f}{\|f\|} = \frac{f_s}{f^\top R e_3} f$$

and one can conclude that

$$f_s = f^\top R e_3.$$

Subsequently, selecting an arbitrary vector $r_{1a} \in \mathbb{R}^3$, which is not parallel to r_{3d} , one can calculate the desired attitude as $R_d(t) = [r_{2d} \times r_{3d}; r_{2d}; r_{3d}]$, where $r_{2d} = \frac{r_{3d} \times r_{1a}}{\|r_{3d} \times r_{1a}\|}$ represents the second row of the desired rotation matrix. The torque control input given in [22] and [23] is used to track the desired attitude, and its form is as follows:

$$\tau = -k_R e_R - k_\Omega e_\Omega + \hat{\Omega} J \Omega - J (\hat{\Omega} R^\top R_d \Omega_d - R^\top R_d \dot{\Omega})$$

where $e_R, e_\Omega \in \mathbb{R}^3$ are attitude and angular velocity errors of the quadrotor. $J \in \mathbb{R}^{3 \times 3}$ is the quadrotor's moment of inertia. $\Omega \in \mathbb{R}^3$ and $\Omega_d \in \mathbb{R}^3$ stand for the angular velocity of the quadrotor in the body-fixed frame and the desired angular velocity of the quadrotor, respectively. $k_R, k_\Omega \in \mathbb{R}$ are positive constants. The hat map $\hat{\cdot} : \mathbb{R}^3 \rightarrow \mathfrak{so}(3)$ is defined by the condition that $\hat{x}y = x \times y$ for all $x, y \in \mathbb{R}^3$. The torque control input is used to ensure that the zero equilibrium of attitude tracking error is exponentially stable, and the proof process can be found in [22].

IV. STABILITY ANALYSIS

In this section, we first prove that the constructed function $E_a(t)$ is positive definite, based on which, theoretical proofs for the main results are further provided.

Theorem 1: The constructed function $E_a(t)$ is positive definite w.r.t. $\Theta_1(t), \Theta_2(t), \dot{\Theta}_1(t)$, and $\dot{\Theta}_2(t)$ for $\Theta_1(t), \Theta_2(t) \in (-\frac{\pi}{2}, \frac{\pi}{2})$.

Proof: To begin with, we reorganize $E_{a2} + E_{a3}$ into the following quadratic form:

$$E_{a2} + E_{a3} = \frac{1}{2} [\dot{\Theta}_1^\top, \dot{\Theta}_2^\top] E_q [\dot{\Theta}_1^\top, \dot{\Theta}_2^\top]^\top \quad (50)$$

where E_q is defined as

$$E_q = \begin{bmatrix} E_{q11} & 0 & E_{q13} & E_{q14} \\ 0 & E_{q22} & E_{q23} & E_{q24} \\ E_{q31} & E_{q32} & E_{q33} & 0 \\ E_{q41} & E_{q42} & 0 & E_{q44} \end{bmatrix} \quad (51)$$

wherein

$$\begin{aligned} E_{q11} &= -m_0 l_1 k_1 C_{1y}^2, E_{q22} = -m_0 l_1 k_1 \\ E_{q33} &= -(m_0 + m_1) l_2 k_2 C_{2y}^2, E_{q44} = -(m_0 + m_1) l_2 k_2 \\ E_{q13} &= E_{q31} = -m_0 l_1 k_2 C_{(1-2)x} C_{1y} C_{2y} \\ E_{q14} &= E_{q41} = -m_0 l_1 k_2 S_{(1-2)x} C_{1y} S_{2y} \\ E_{q23} &= E_{q32} = m_0 l_1 k_2 S_{(1-2)x} S_{1y} C_{2y} \\ E_{q24} &= E_{q42} = -m_0 l_1 k_2 (C_{(1-2)x} S_{1y} S_{2y} + C_{1y} C_{2y}). \end{aligned}$$

The determinant of the leading principal minors of E_q are given by

$$\Delta_1 = -m_0 l_1 k_1 C_{1y}^2, \Delta_2 = m_0^2 l_1^2 k_1^2 C_{1y}^2 \quad (52)$$

$$\Delta_3 = m_0^3 l_1^3 k_1 k_2 C_{(1-2)x}^2 C_{1y}^2 C_{2y}^2 + m_0^3 l_1^3 k_1 k_2 S_{(1-2)x}^2 C_{1y}^2 S_{1y}^2.$$

$$C_{2y}^2 - m_0^2 (m_0 + m_1) l_1^2 l_2 k_1^2 k_2 C_{1y}^2 C_{2y}^2 \quad (53)$$

$$\Delta_4 = \alpha_1 C_{1y}^2 C_{2y}^2 - \alpha_2 [C_{(1-2)x} C_{1y}^2 C_{2y}^2 + C_{1y} S_{1y} C_{2y} S_{2y}]^2 \quad (54)$$

where

$$\begin{aligned} \alpha_1 &= [m_0^2 (m_0 + m_1)^2 l_1^2 l_2 k_1^2 k_2^2 - m_0^3 (m_0 + m_1) l_1^3 l_2 k_1 k_2^3] \\ \alpha_2 &= [m_0^3 (m_0 + m_1) l_1^3 l_2 k_1 k_2^3 - m_0^4 l_1^4 k_2^4]. \end{aligned} \quad (55)$$

As control gains $k_1, k_2 < 0$, it is obvious that

$$\Delta_1, \Delta_2 > 0. \quad (56)$$

Then, we will further demonstrate that Δ_3 and Δ_4 are positive. By utilizing (39), we can obtain

$$\begin{aligned} \Delta_3 &= m_0^3 l_1^3 k_1 k_2 C_{(1-2)x}^2 C_{1y}^2 C_{2y}^2 + m_0^3 l_1^3 k_1 k_2 S_{(1-2)x}^2 C_{1y}^2 S_{1y}^2 \\ &\quad C_{2y}^2 - m_0^2 (m_0 + m_1) \left(1 + \frac{m_1}{m_2}\right) l_1^3 k_1 k_2^2 C_{1y}^2 C_{2y}^2 \\ &= -\frac{m_0^2 (m_0 m_1 + m_1^2 + m_1 m_2)}{m_2} l_1^3 k_1 k_2^2 C_{1y}^2 C_{2y}^2 \\ &\quad - m_0^3 l_1^3 k_1 k_2^2 S_{(1-2)x}^2 C_{1y}^4 C_{2y}^2 > 0. \end{aligned} \quad (57)$$

In an analogous manner, one has

$$\begin{aligned} C_{1y}^2 C_{2y}^2 &\geq [C_{(1-2)x} C_{1y}^2 C_{2y}^2 + C_{1y} S_{1y} C_{2y} S_{2y}]^2 \\ \alpha_1 &> \alpha_2 > 0 \Rightarrow \Delta_4 > 0 \end{aligned} \quad (58)$$

where the first inequality of (58) is satisfied locally according to *Assumption 1*. As each of its determinant of the leading principal minors is positive, symmetric matrix E_q is locally positive definite. Combining $\Delta_1, \Delta_2, \Delta_3, \Delta_4 > 0$ and the result of (37), it is clear that $E_a(t)$ is positive definite according to *Assumption 1*. ■

Theorem 2: Under the proposed enhanced-coupling control scheme given by (48), the equilibrium point of the corresponding closed-loop system is local asymptotically stable, and the error signal $e_\xi(t)$ and the hook/cargo swing angels $\theta_{1x}(t), \theta_{1y}(t), \theta_{2x}(t)$, and $\theta_{2y}(t)$ converge to zero, that is

$$\lim_{t \rightarrow \infty} e_\xi(t) = \mathbf{0}, \lim_{t \rightarrow \infty} \theta_{1x}(t), \theta_{1y}(t), \theta_{2x}(t), \theta_{2y}(t) = 0. \quad (59)$$

Proof: Consider $V(t)$ constructed in (46) as the Lyapunov function candidate. It is straightforward from (14), (24), and the result in *Theorem 1* that $V(t)$ is positive definite w.r.t. $e_\gamma(t), \dot{\xi}(t), \Theta_1(t), \Theta_2(t), \dot{\Theta}_1(t)$, and $\dot{\Theta}_2(t)$ on the span of $\Theta_1(t), \Theta_2(t) \in (-\frac{\pi}{2}, \frac{\pi}{2})$. Then, substituting (48) into (47), we are led to the following result:

$$\dot{V} = -\dot{e}_\gamma^\top K_d \tanh(\dot{e}_\gamma) \leq 0 \quad (60)$$

which directly implies that

$$V \in \mathcal{L}_\infty \Rightarrow e_\gamma, e_\xi, \gamma, \dot{\xi}, \dot{e}_\gamma, \dot{\gamma}, \dot{\Theta}_1, \dot{\Theta}_2 \in \mathcal{L}_\infty. \quad (61)$$

Further, define Γ as the largest invariant set with Φ , and Φ is the set where $\dot{V}(t) = 0$, that is

$$\Phi \triangleq \left\{ (e_\xi, \Theta_1, \Theta_2, \dot{e}_\xi, \dot{\Theta}_1, \dot{\Theta}_2) : \dot{V} = 0 \right\}. \quad (62)$$

It is then deduced that

$$\dot{e}_\gamma = \mathbf{0} \Rightarrow e_\gamma = \mu_\gamma, \ddot{e}_\gamma = \mathbf{0} \quad (63)$$

with $\mu_\gamma = [\mu_{\gamma x}, \mu_{\gamma y}, \mu_{\gamma z}]^\top$ being a constant vector to be determined, and the control input u_f takes the following expression:

$$u_f = -K_p \tanh(\mu_\gamma). \quad (64)$$

The proof process is divided into two steps.

Step 1: Recalling (1)–(3), one has

$$\begin{aligned} (m_0 + m_1 + m_2) \ddot{x} + (m_1 + m_2) l_1 \frac{d}{dt} \omega_{11} + m_2 l_2 \frac{d}{dt} \omega_{12} = \\ -k_{px} \tanh(\mu_{\gamma x}) \end{aligned} \quad (65)$$

$$\begin{aligned} (m_0 + m_1 + m_2) \ddot{y} + (m_1 + m_2) l_1 \frac{d}{dt} \omega_{21} + m_2 l_2 \frac{d}{dt} \omega_{22} = \\ -k_{py} \tanh(\mu_{\gamma y}) \end{aligned} \quad (66)$$

$$\begin{aligned} (m_0 + m_1 + m_2) \ddot{z} + (m_1 + m_2) l_1 \frac{d}{dt} \omega_{31} + m_2 l_2 \frac{d}{dt} \omega_{32} = \\ -k_{pz} \tanh(\mu_{\gamma z}). \end{aligned} \quad (67)$$

where auxiliary terms $\omega_{11}, \omega_{12}, \omega_{21}, \omega_{22}, \omega_{31}$, and ω_{32} are defined as

$$\omega_{11} = \dot{\theta}_{1x} C_{1x} C_{1y} - \dot{\theta}_{1y} S_{1x} S_{1y}, \omega_{12} = \dot{\theta}_{2x} C_{2x} C_{2y} - \dot{\theta}_{2y} S_{2x} S_{2y} \quad (68)$$

$$\omega_{21} = \dot{\theta}_{1y} C_{1y}, \omega_{22} = \dot{\theta}_{2y} C_{2y} \quad (69)$$

$$\omega_{31} = \dot{\theta}_{1x} S_{1x} C_{1y} + \dot{\theta}_{1y} C_{1x} S_{1y}, \omega_{32} = \dot{\theta}_{2x} S_{2x} C_{2y} + \dot{\theta}_{2y} C_{2x} S_{2y}. \quad (70)$$

From (61), one can derive that

$$\omega_{11}, \omega_{12}, \omega_{21}, \omega_{22}, \omega_{31}, \omega_{32} \in \mathcal{L}_\infty. \quad (71)$$

With conclusions in (42)–(44) and (63) yields

$$\ddot{e}_x + k_1 \frac{d}{dt} \omega_{11} + k_2 \frac{d}{dt} \omega_{12} = 0 \quad (72)$$

$$\ddot{e}_y + k_1 \frac{d}{dt} \omega_{21} + k_2 \frac{d}{dt} \omega_{22} = 0 \quad (73)$$

$$\ddot{e}_z + k_1 \frac{d}{dt} \omega_{31} + k_2 \frac{d}{dt} \omega_{32} = 0. \quad (74)$$

By substituting (72)–(74) into (65)–(67), the following results are obtained:

$$[(m_0 + m_1 + m_2) k_1 - (m_1 + m_2) l_1] \frac{d}{dt} \omega_{11} \\ + [(m_0 + m_1 + m_2) k_2 - m_2 l_2] \frac{d}{dt} \omega_{12} = k_{px} \mu_{\gamma x} \quad (75)$$

$$[(m_0 + m_1 + m_2) k_1 - (m_1 + m_2) l_1] \frac{d}{dt} \omega_{21} \\ + [(m_0 + m_1 + m_2) k_2 - m_2 l_2] \frac{d}{dt} \omega_{22} = k_{py} \mu_{\gamma y} \quad (76)$$

$$[(m_0 + m_1 + m_2) k_1 - (m_1 + m_2) l_1] \frac{d}{dt} \omega_{31} \\ + [(m_0 + m_1 + m_2) k_2 - m_2 l_2] \frac{d}{dt} \omega_{32} = k_{pz} \mu_{\gamma z}. \quad (77)$$

Assuming that $\mu_{\gamma x} \neq 0$, $\mu_{\gamma y} \neq 0$, and $\mu_{\gamma z} \neq 0$, integrating both sides of (75)–(77), respectively, leads to

$$[(m_0 + m_1 + m_2) k_1 - (m_1 + m_2) l_1] \omega_{11} \\ + [(m_0 + m_1 + m_2) k_2 - m_2 l_2] \omega_{12} = k_{px} \mu_{\gamma x} t + v_{1x} \quad (78)$$

$$[(m_0 + m_1 + m_2) k_1 - (m_1 + m_2) l_1] \omega_{21} \\ + [(m_0 + m_1 + m_2) k_2 - m_2 l_2] \omega_{22} = k_{py} \mu_{\gamma y} t + v_{1y} \quad (79)$$

$$[(m_0 + m_1 + m_2) k_1 - (m_1 + m_2) l_1] \omega_{31} \\ + [(m_0 + m_1 + m_2) k_2 - m_2 l_2] \omega_{32} = k_{pz} \mu_{\gamma z} t + v_{1z} \quad (80)$$

where $\mathbf{v}_1 = [v_{1x}, v_{1y}, v_{1z}]^\top$ is a constant vector to be determined. Thus, the left-hand sides of (78)–(80) may tend to infinity, which conflicts with the aforementioned boundedness conclusions for ω_{11} , ω_{12} , ω_{21} , ω_{22} , ω_{31} , and ω_{32} as given in (71). Hence, together with (63) and (64), one can conclude that

$$\boldsymbol{\mu}_\gamma = \mathbf{0} \Rightarrow \dot{\mathbf{e}}_\gamma = \mathbf{0}, \mathbf{u}_f = \mathbf{0}. \quad (81)$$

Substituting the results in (81) into (75)–(77), and comparing it with (72)–(74) upon using (39), it can be deduced that

$$\ddot{\mathbf{e}}_\xi = \mathbf{0} \Rightarrow \dot{\mathbf{e}}_\xi = \boldsymbol{\mu}_\xi \quad (82)$$

with $\boldsymbol{\mu}_\xi = [\mu_{\xi x}, \mu_{\xi y}, \mu_{\xi z}]^\top$ being a constant vector. Analogously, if $\mu_{\xi x} \neq 0$, $\mu_{\xi y} \neq 0$, and $\mu_{\xi z} \neq 0$, then $e_x(t)$, $e_y(t)$, $e_z(t) \rightarrow \infty$, which leads to an apparent contradiction due to the result $\mathbf{e}_\xi \in \mathcal{L}_\infty$ in (61). Thus, the following results is concluded:

$$\boldsymbol{\mu}_\xi = \mathbf{0} \Rightarrow \dot{\mathbf{e}}_\xi = \mathbf{0}. \quad (83)$$

Step 2: Substituting (81) and (82) into (1)–(3) and (5), and combining these four formulas, the following equation can be obtained:

$$(m_1 + m_2) g l_1 C_{1x} S_{1y} = 0 \quad (84)$$

and combined with (9), the following result is derived:

$$S_{1y} = 0 \Rightarrow \theta_{1y} = 0, \dot{\theta}_{1y} = 0, \ddot{\theta}_{1y} = 0. \quad (85)$$

Substituting (82) into (66), and integrating both sides of the derived result with respect to time, one can obtain

$$(m_1 + m_2) l_1 \omega_{21} + m_2 l_2 \omega_{22} = -k_{py} \tanh(\mu_{\gamma y}) t + v_{2y} \quad (86)$$

where v_{2y} is a constant yet to be decided. Then, combining (81), (85), and (86), one can derive that $m_2 l_2 (\dot{\theta}_{2y} C_{2y}) = v_{2y}$, which can be rewritten as $\frac{d}{dt} S_{2y} = \frac{v_{2y}}{m_2 l_2}$, the integral of above equation with respect to time can be presented as $S_{2y} = \frac{v_{2y}}{m_2 l_2} t + v_{S_{2y}}$, with $v_{S_{2y}}$ representing a yet-to-be-determined constant number. Further, assuming that $v_{2y} \neq 0$, if $t \rightarrow \infty$, S_{2y} tends to infinity, which conflicts with the fact that $S_{2y} \in (-1, 1)$. Accordingly, the following result is derived:

$$v_{2y} = 0, S_{2y} = v_{S_{2y}} \Rightarrow \dot{\theta}_{2y} = 0, \ddot{\theta}_{2y} = 0. \quad (87)$$

Substituting (81), (82), (85), and (87) into (1), (3)–(4), and (6)–(7), the following formulas can be obtained:

$$(m_1 + m_2) l_1 \left(\ddot{\theta}_{1x} C_{1x} - \dot{\theta}_{1x}^2 S_{1x} \right) + m_2 l_2 \left(\ddot{\theta}_{2x} C_{2x} C_{2y} \right. \\ \left. - \dot{\theta}_{2x}^2 S_{2x} C_{2y} \right) = 0 \quad (88)$$

$$(m_1 + m_2) l_1 \left(\ddot{\theta}_{1x} S_{1x} + \dot{\theta}_{1x}^2 C_{1x} \right) + m_2 l_2 \left(\ddot{\theta}_{2x} S_{2x} C_{2y} \right. \\ \left. + \dot{\theta}_{2x}^2 C_{2x} C_{2y} \right) = 0 \quad (89)$$

$$(m_1 + m_2) l_1^2 \ddot{\theta}_{1x} + m_2 l_1 l_2 C_{2y} \left(\ddot{\theta}_{2x} C_{(1-2)x} + \dot{\theta}_{2x}^2 S_{(1-2)x} \right) \\ + (m_1 + m_2) g l_1 S_{1x} = 0 \quad (90)$$

$$m_2 l_2^2 \ddot{\theta}_{2x} C_{2y}^2 + m_2 l_1 l_2 C_{2y} \left(\ddot{\theta}_{1x} C_{(1-2)x} - \dot{\theta}_{1x}^2 S_{(1-2)x} \right) \\ + m_2 g l_2 S_{2x} C_{2y} = 0 \quad (91)$$

$$m_2 l_2^2 \dot{\theta}_{2x}^2 C_{2y} S_{2y} + m_2 l_1 l_2 S_{2y} \left(\ddot{\theta}_{1x} S_{(1-2)x} + \dot{\theta}_{1x}^2 C_{(1-2)x} \right) \\ + m_2 g l_2 C_{2x} S_{2y} = 0. \quad (92)$$

By using (88)–(90), and according to (9), after some mathematical manipulation, one can conclude that

$$(m_1 + m_2) g l_1 S_{1x} = 0 \Rightarrow S_{1x} = 0 \\ \Rightarrow \theta_{1x} = 0, \dot{\theta}_{1x} = 0, \ddot{\theta}_{1x} = 0. \quad (93)$$

Then, substituting (93) into (88) and (89), we derive $m_2 l_2 \dot{\theta}_{2x} C_{2y} = 0$, which together with (9) leads to $\dot{\theta}_{2x} = 0$. Similarly, substituting (93) and $\dot{\theta}_{2x} = 0$ into (91), the following results are obvious:

$$m_2 g l_2 S_{2x} C_{2y} = 0 \Rightarrow S_{2x} = 0, \theta_{2x} = 0, \dot{\theta}_{2x} = 0. \quad (94)$$

Next, with the result in (93) and (94), from (92), one can make some arrangements to derive

$$m_2 g l_2 C_{2x} S_{2y} = 0 \Rightarrow S_{2y} = 0, \theta_{2y} = 0. \quad (95)$$

Accordingly, combining the result in (81), (85), (93), (94), and (95) into (42)–(44), one can get

$$e_x = 0, e_y = 0, e_z = 0. \quad (96)$$

TABLE I
QUANTITATIVE DATA

	max				RMS				rise time			
	θ_{1x}	θ_{1y}	θ_{2x}	θ_{2y}	θ_{1x}	θ_{1y}	θ_{2x}	θ_{2y}	x	y	z	
Exp 1	PD controller	24.0°	26.5°	40.8°	37.1°	5.6°	5.7°	8.5°	8.1°	3.8 s	3.1 s	2.3 s
	LQR controller	20.0°	22.6°	33.3°	36.1°	4.5°	5.4°	6.5°	9.0°	5.0 s	3.5 s	1.9 s
	controller given in [28]	17.0°	23.0°	27.4°	28.3°	3.8°	6.1°	6.1°	7.6°	5.2 s	3.8 s	2.5 s
	proposed controller	16.1°	15.2°	22.3°	17.3°	3.3°	3.0°	4.8°	4.1°	3.6 s	3.3 s	2.1 s
Exp 2	PD controller	26.1°	25.1°	51.5°	38.4°	6.9°	7.9°	11.8°	12.3°	3.3 s	6.4 s	2.5 s
	LQR controller	25.5°	26.8°	41.6°	33.6°	5.8°	8.2°	9.4°	11.0°	3.5 s	7.1 s	1.8 s
	controller given in [28]	27.1°	24.3°	33.5°	33.1°	6.7°	6.4°	9.0°	8.4°	3.7 s	7.3 s	2.6 s
	proposed controller	12.8°	14.2°	16.2°	20.7°	3.0°	3.6°	3.8°	5.3°	3.0 s	5.7 s	2.2 s

TABLE II
RMS OF THE CONTROL ACTIONS FOR EXPERIMENT 1

Exp 1	RMS		
	f_x	f_y	f_z
PD controller	0.71 N	0.91 N	15.88 N
LQR controller	0.58 N	0.82 N	15.90 N
controller given in [28]	0.61 N	0.83 N	15.83 N
proposed controller	0.58 N	0.60 N	15.86 N

By summarizing the conclusions of (83), (85), and (93)–(96), it is known that the largest invariant set Γ only contains the equilibrium point, i.e.

$$\Gamma = \left\{ \left(e_\xi, \Theta_1, \Theta_2, \dot{e}_\xi, \dot{\Theta}_1, \dot{\Theta}_2 \right) : e_\xi, \Theta_1, \Theta_2, \dot{e}_\xi, \dot{\Theta}_1, \dot{\Theta}_2 = 0 \right\}.$$

Hereto, by invoking LaSalle's Invariance Theorem [34], the proof is completed. ■

Remark 3: According to the hierarchical control scheme in [3] and [23], the feature of coupling term will be discussed in order to guarantee the stability of the closed-loop system. Based on the result in *Remark 2*, it can be deduced that $\Delta = \|f\|[(e_3^\top R_d^\top R e_3) R e_3 - R_d e_3]$. According to the geometric analysis in [22] and the theory on cascade systems in [3] and [23], it can be proved that the coupling term satisfies the growth restriction condition, thus the asymptotic convergence of the overall system is guaranteed.

V. HARDWARE EXPERIMENTS

In this section, we implement two groups of experiments to validate the performance of the proposed control method, including tests to observe the control performance in robustness validation with comparative methods.

As shown in Fig. 3, the experiments are carried out on the testbed consisting of the quadrotor transportation system, the Qualisys motion capture system, the ground station, and the onboard Raspberry Pi. AIR2216-880kv motors are utilized to provide flight power for the quadrotor with a wingspan of 450 mm. The Qualisys motion capture system, which includes eight cameras, is used to measure the state signals of the quadrotor and the swing angles by identifying the markers on the quadrotor, the hook, and the cargo. The ground station receives data from motion capture via local area network and transmits

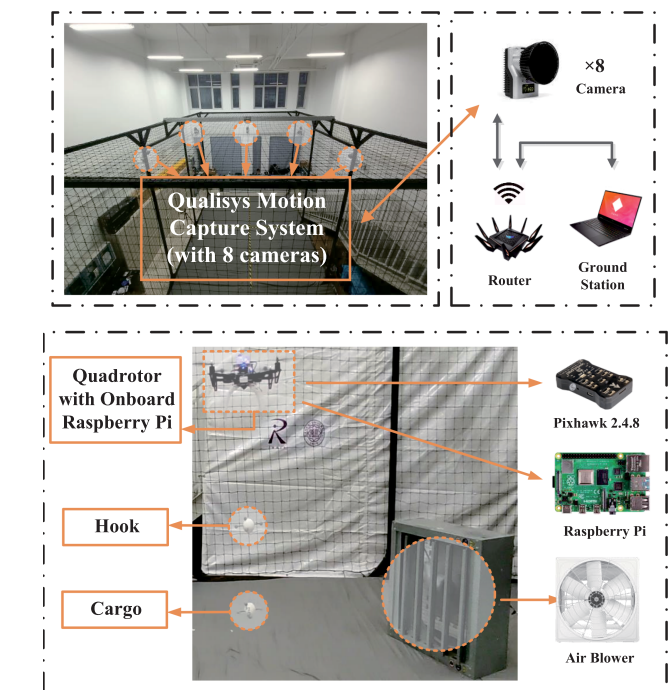


Fig. 3. Experiment testbed.

control signals to the computer stick via WIFI with 5G band. The Raspberry Pi runs the 64-bit Ubuntu 18.04 operating system, and it is connected to the quadrotor's flight controller PixHawk by MAVROS-based communication protocol. It is worthwhile to mention that the data interactions in the project are supported by the communication protocol of Robot Operating System. The parameters of the testbed are provided as

$$m_0 = 1.45\text{kg}, m_1 = 0.10\text{kg}, m_2 = 0.05\text{kg}$$

$$l_1 = 0.6\text{m}, l_2 = 0.3\text{m}, g = 9.8\text{kg} \cdot \text{m/s}^2$$

$$J = \text{diag}([0.0117, 0.0120, 0.0184])\text{kg} \cdot \text{m}^2.$$

To validate the performance of the proposed method in quadrotor positioning and swing suppression, the proposed controller is compared with the proportional-derivative (PD) regulation controller, the linear quadratic regulator (LQR) controller and the controller proposed in [28]. After a large amount

TABLE III
REDUCTION RATIO ON SWING ANGLES

comparison method		reduction ratio on max				reduction ratio on RMS			
		θ_{1x}	θ_{1y}	θ_{2x}	θ_{2y}	θ_{1x}	θ_{1y}	θ_{2x}	θ_{2y}
Exp 1	PD controller	32.9%	42.6%	45.3%	53.4%	41.1%	47.4%	43.5%	49.4%
	LQR controller	19.5%	32.7%	33.0%	52.1%	26.7%	44.4%	26.2%	54.4%
	controller given in [28]	5.3%	33.9%	18.6%	38.9%	13.2%	50.8%	21.3%	46.1%
Exp 2	PD controller	51.0%	43.4%	68.5%	46.1%	56.5%	54.4%	67.8%	56.9%
	LQR controller	49.8%	47.0%	61.1%	38.4%	48.3%	56.1%	59.6%	51.8%
	controller given in [28]	52.8%	41.6%	51.6%	37.5%	55.2%	43.8%	57.8%	36.9%

of literature investigation, we failed to find other nonlinear control methods for aerial transportation systems with 3-D double-pendulum swing effects except the method given in [28]. Therefore, in addition to the nonlinear method given in [28], the classical PD algorithm and LQR algorithm are chosen as the comparative method. Numerical simulation tests are performed to validate the performance of the proposed controller before experiments, and we repeat the practical experiment a couple of times to tune the control parameters with experience. By evaluating the effects of overshoot avoidance and swing suppression, the control gains for the proposed enhanced-coupling controller are chosen as

$$\begin{aligned} k_{px} &= k_{py} = 4.8, k_{pz} = 8.0, k_{dx} = k_{dy} = 6.0, k_{dz} = 10.0 \\ k_1 &= -0.17, k_2 = -0.03. \end{aligned}$$

The PD controller is given as

$$\begin{aligned} f_x &= -k_{px}e_x - k_{dx}\dot{e}_x \\ f_y &= -k_{py}e_y - k_{dy}\dot{e}_y \\ f_z &= -k_{pz}e_z - k_{dz}\dot{e}_z + (m_0 + m_1 + m_2)g \end{aligned}$$

where the control gains of the PD controller are set as: $k_{px} = k_{py} = 4.5$, $k_{pz} = 7.0$, $k_{dx} = k_{dy} = 6.0$, and $k_{dz} = 10.0$.

The form of the LQR controller is as follows:

$$\begin{aligned} f_x &= -k_1^L e_x - k_2^L \theta_{1x} - k_3^L \theta_{2x} - k_4^L \dot{e}_x - k_5^L \dot{\theta}_{1x} - k_6^L \dot{\theta}_{2x} \\ f_y &= -k_7^L e_y - k_8^L \theta_{1y} - k_9^L \theta_{2y} - k_{10}^L \dot{e}_y - k_{11}^L \dot{\theta}_{1y} - k_{12}^L \dot{\theta}_{2y} \\ f_z &= -k_{13}^L e_z - k_{14}^L \dot{e}_z + (m_0 + m_1 + m_2)g. \end{aligned}$$

Control gains of the LQR controller $k_1^L = k_7^L = 4.0$, $k_2^L = k_8^L = -0.173$, $k_3^L = k_9^L = 0.066$, $k_4^L = k_{10}^L = 6.0$, $k_5^L = k_{11}^L = 0.023$, $k_6^L = k_{12}^L = 0.025$, $k_{13}^L = 7.0$, and $k_{14}^L = 10.0$ can be obtained by MATLAB toolbox.

The controller mentioned in [28] that involves signals about both the quadrotor's position and the double-pendulum swing angles, as follows:

$$\begin{aligned} f_x &= -k_{px}e_x - k_{dx}\dot{e}_x - k_x(\dot{\theta}_{1x}^2 + \dot{\theta}_{1y}^2 + \dot{\theta}_{2x}^2 + \dot{\theta}_{2y}^2)\dot{e}_x \\ f_y &= -k_{py}e_y - k_{dy}\dot{e}_y - k_y(\dot{\theta}_{1x}^2 + \dot{\theta}_{1y}^2 + \dot{\theta}_{2x}^2 + \dot{\theta}_{2y}^2)\dot{e}_y \\ f_z &= -k_{pz}e_z - k_{dz}\dot{e}_z - k_z(\dot{\theta}_{1x}^2 + \dot{\theta}_{1y}^2 + \dot{\theta}_{2x}^2 + \dot{\theta}_{2y}^2)\dot{e}_z \end{aligned}$$

TABLE IV
RMS OF THE CONTROL ACTIONS FOR EXPERIMENT 2

Exp 2	RMS		
	f_x	f_y	f_z
PD controller	0.79 N	0.95 N	15.83 N
LQR controller	0.70 N	0.91 N	15.88 N
controller given in [28]	0.76 N	0.96 N	15.87 N
proposed controller	0.70 N	0.90 N	15.82 N

$$+ (m_0 + m_1 + m_2)g$$

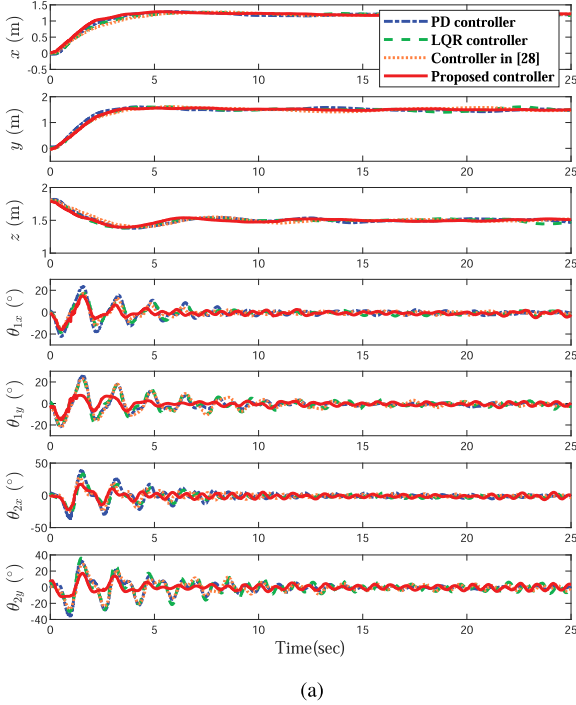
where the control gains are set to be $k_{px} = k_{py} = 3.8$, $k_{pz} = 7.0$, $k_{dx} = k_{dy} = 6.3$, $k_{dz} = 10.0$, and $k_x = k_y = k_z = 0.3$.

A. Experiment 1—Control Performance Validation

The initial position and desired position of the quadrotor are set as $\xi = [0, 0, 1.8]^\top$ m and $\xi_d = [1.2, 1.5, 1.5]^\top$ m, respectively. Results of the quadrotor position ξ and the swing angles Θ_1 and Θ_2 for all the four methods are provided in Fig. 4. From Fig. 4, one can see that all the four methods could drive the quadrotor to the desired position with similar positioning accuracy, and the proposed one could suppress the swing motion of the hook and the cargo more effectively. The maximum values of the double-pendulum swing angles are related to the speed of the quadrotor as it flies toward the desired position. In order to ensure a more fair comparison of the four methods, we have made their rise times at the same level as much as possible, which are given in Table I. The root mean square (RMS) values of the control actions are provided in Table II, which indicate that the proposed controller demands similar control effort. Moreover, Table I illustrates the maximum and RMS values of double-pendulum swing angles in the experiments, from which one can find that the swing angles' maximum and RMS values of the proposed method are obviously smaller than those of the other three methods. Besides, define the reduction ratio on swing angles of the proposed method compared with the three comparison methods as

$$\text{Ratio} = \frac{\theta_i[\text{Com.}] - \theta_i[\text{Pro.}]}{\theta_i[\text{Com.}]}$$

where i denotes $1x$, $1y$, $2x$, and $2y$, Com. represents for the comparison method, and Pro. is the proposed method. The



(a)

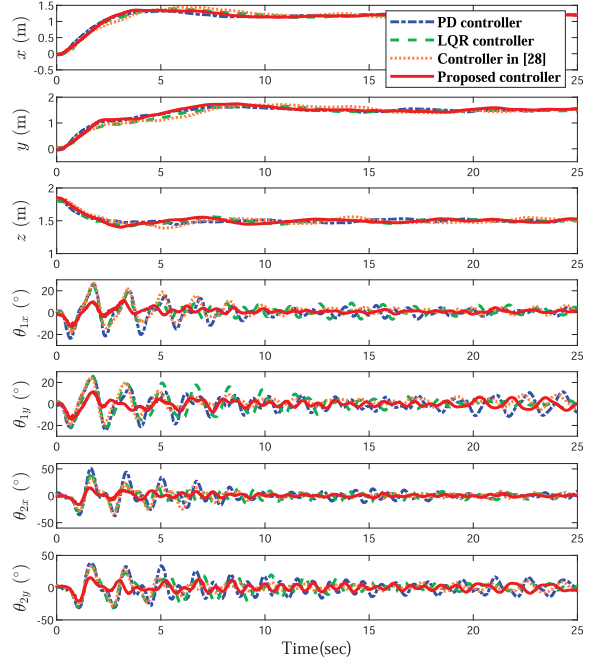
(b)

Fig. 4. Results for Experiment 1. (a) Quadrotor positions and cargo/hook swing angles. (b) Outer loop control input components in x , y , and z directions.

calculated result is provided in Table III, which demonstrates the superior antiswing performance of the proposed method.

B. Experiment 2—Robustness Verification Experiment

As shown in Fig. 3, an air blower is used to impose continuous wind disturbance on the system to verify the control performance of the proposed method under a more harsh condition. Fig. 5 and Table I show the results of the wind disturbance experiment, by comparing them with the results of Experiment 1, it can be concluded that the positioning performance of the quadrotor is significantly worse under the influence of wind interference. In this case, all the four methods can still make the quadrotor aircraft achieve a satisfactory positioning state. It



(a)

(b)

Fig. 5. Results for Experiment 2. (a) Quadrotor positions and cargo/hook swing angles. (b) Outer loop control input components in x , y , and z directions.

is notable that the proposed controller requires similar control effort while achieving better antiswing performance than the other three controllers, as given in Table IV. Thus, the superiority of the proposed method is validated.

Remark 4: This article focuses on the improvement of the antiswing performance for the aerial transportation system with double-pendulum swing effects. Under the control framework in this article, it is difficult to obtain the unbiased estimation of the cargo mass since the persistent-excitation condition [35] cannot be satisfied. Therefore, the convergence of the quadrotor positioning in the vertical direction is hard to be guaranteed theoretically, which is still a problem that needs to be solved. In future work, we will further design more advanced control

methods to cope with the variation of the cargo, such as modeling cargo variation, or regarding it as disturbance to design corresponding robust control schemes.

VI. CONCLUSION

In this article, based on energy analysis, a novel enhanced-coupling controller for the quadrotor positioning and double-pendulum swing angle elimination is proposed for aerial transportation systems. Specifically, after the basic energy analysis, cargo and hook information are introduced in the error term and the energy storage function. It is worth mentioning that the state coupling between the translational motion of the quadrotor and the cargo/hook motion is strengthened, hence, the transient performance of the enhanced-coupling controller is improved. Then, Lyapunov-based analysis is provided to prove the stability of the closed-loop system. As recorded by experimental data, the proposed method presents superior control performance and satisfactory robustness. In future efforts, constraint control for both the hook and the cargo will be considered to theoretically ensure that the swing angles are always within the constraint. In consideration of the passive characteristics of the controller, adding nonlinear integral terms to improve controlling performance with guaranteed stability analysis will be implemented in future work.

APPENDIX

The inertia matrix $M(\mathbf{q})$ is defined as

$$M(\mathbf{q}) = \begin{bmatrix} M_{11} & 0 & 0 & M_{14} & M_{15} & M_{16} & M_{17} \\ 0 & M_{22} & 0 & 0 & M_{25} & 0 & M_{27} \\ 0 & 0 & M_{33} & M_{34} & M_{35} & M_{36} & M_{37} \\ M_{41} & 0 & M_{43} & M_{44} & 0 & M_{46} & M_{47} \\ M_{51} & M_{52} & M_{53} & 0 & M_{55} & M_{56} & M_{57} \\ M_{61} & 0 & M_{63} & M_{64} & M_{65} & M_{66} & 0 \\ M_{71} & M_{72} & M_{73} & M_{74} & M_{75} & 0 & M_{77} \end{bmatrix}$$

where

$$M_{11} = M_{22} = M_{33} = m_0 + m_1 + m_2$$

$$M_{44} = (m_1 + m_2) l_1^2 C_{1y}^2, M_{55} = (m_1 + m_2) l_1^2$$

$$M_{66} = m_2 l_2^2 C_{2y}^2, M_{77} = m_2 l_2^2$$

$$M_{14} = M_{41} = (m_1 + m_2) l_1 C_{1x} C_{1y}$$

$$M_{15} = M_{51} = -(m_1 + m_2) l_1 S_{1x} S_{1y}$$

$$M_{16} = M_{61} = m_2 l_2 C_{2x} C_{2y}, M_{17} = M_{71} = -m_2 l_2 S_{2x} S_{2y}$$

$$M_{25} = M_{52} = (m_1 + m_2) l_1 C_{1y}, M_{27} = M_{72} = m_2 l_2 C_{2y}$$

$$M_{34} = M_{43} = (m_1 + m_2) l_1 S_{1x} C_{1y}$$

$$M_{35} = M_{53} = (m_1 + m_2) l_1 C_{1x} S_{1y}$$

$$M_{36} = M_{63} = m_2 l_2 S_{2x} C_{2y}, M_{37} = M_{73} = m_2 l_2 C_{2x} S_{2y}$$

$$M_{46} = M_{64} = m_2 l_1 l_2 C_{1y} C_{2y} C_{(1-2)x}$$

$$M_{47} = M_{74} = m_2 l_1 l_2 C_{1y} S_{2y} S_{(1-2)x}$$

$$M_{56} = M_{65} = -m_2 l_1 l_2 S_{1y} C_{2y} S_{(1-2)x}$$

$$M_{57} = M_{75} = m_2 l_1 l_2 (C_{1y} C_{2y} + S_{1y} S_{2y} C_{(1-2)x}).$$

The centrifugal and Coriolis matrix $V_c \in \mathbb{R}^{7 \times 7}$ is defined by

$$V_{c14} = -(m_1 + m_2) l_1 (\dot{\theta}_{1x} S_{1x} C_{1y} + \dot{\theta}_{1y} C_{1x} S_{1y})$$

$$V_{c15} = -(m_1 + m_2) l_1 (\dot{\theta}_{1x} C_{1x} S_{1y} + \dot{\theta}_{1y} S_{1x} C_{1y})$$

$$V_{c16} = -m_2 l_2 (\dot{\theta}_{2x} S_{2x} C_{2y} + \dot{\theta}_{2y} C_{2x} S_{2y})$$

$$V_{c17} = -m_2 l_2 (\dot{\theta}_{2x} C_{2x} S_{2y} + \dot{\theta}_{2y} S_{2x} C_{2y})$$

$$V_{c25} = -(m_1 + m_2) l_1 \dot{\theta}_{1y} S_{1y}, V_{c27} = -m_2 l_2 \dot{\theta}_{2y} S_{2y}$$

$$V_{c34} = (m_1 + m_2) l_1 (\dot{\theta}_{1x} C_{1x} C_{1y} - \dot{\theta}_{1y} S_{1x} S_{1y})$$

$$V_{c35} = (m_1 + m_2) l_1 (-\dot{\theta}_{1x} S_{1x} S_{1y} + \dot{\theta}_{1y} C_{1x} C_{1y})$$

$$V_{c36} = m_2 l_2 (\dot{\theta}_{2x} C_{2x} C_{2y} - \dot{\theta}_{2y} S_{2x} S_{2y})$$

$$V_{c37} = m_2 l_2 (-\dot{\theta}_{2x} S_{2x} S_{2y} + \dot{\theta}_{2y} C_{2x} C_{2y})$$

$$V_{c44} = -(m_1 + m_2) l_1^2 \dot{\theta}_{1y} C_{1y} S_{1y}$$

$$V_{c45} = -(m_1 + m_2) l_1^2 \dot{\theta}_{1x} C_{1y} S_{1y}$$

$$V_{c46} = m_2 l_1 l_2 C_{1y} (\dot{\theta}_{2x} C_{2y} S_{(1-2)x} - \dot{\theta}_{2y} S_{2y} C_{(1-2)x})$$

$$V_{c47} = m_2 l_1 l_2 C_{1y} (\dot{\theta}_{2y} C_{2y} S_{(1-2)x} - \dot{\theta}_{2x} S_{2y} C_{(1-2)x})$$

$$V_{c54} = (m_1 + m_2) l_1^2 \dot{\theta}_{1x} C_{1y} S_{1y}$$

$$V_{c56} = m_2 l_1 l_2 (\dot{\theta}_{2x} S_{1y} C_{2y} C_{(1-2)x} + \dot{\theta}_{2y} S_{1y} S_{2y} S_{(1-2)x})$$

$$V_{c57} = m_2 l_1 l_2 \left[\dot{\theta}_{2y} (S_{1y} C_{2y} C_{(1-2)x} - C_{1y} S_{2y}) \right. \\ \left. + \dot{\theta}_{2x} S_{1y} S_{2y} S_{(1-2)x} \right]$$

$$V_{c64} = m_2 l_1 l_2 C_{2y} (-\dot{\theta}_{1x} C_{1y} S_{(1-2)x} - \dot{\theta}_{1y} S_{1y} C_{(1-2)x})$$

$$V_{c65} = m_2 l_1 l_2 C_{2y} (-\dot{\theta}_{1y} C_{1y} S_{(1-2)x} - \dot{\theta}_{1x} S_{1y} C_{(1-2)x})$$

$$V_{c66} = -m_2 l_2^2 \dot{\theta}_{2y} C_{2y} S_{2y}, V_{c67} = -m_2 l_2^2 \dot{\theta}_{2x} C_{2y} S_{2y}$$

$$V_{c74} = m_2 l_1 l_2 (\dot{\theta}_{1x} C_{1y} S_{2y} C_{(1-2)x} - \dot{\theta}_{1y} S_{1y} S_{2y} S_{(1-2)x})$$

$$V_{c75} = m_2 l_1 l_2 \left[\dot{\theta}_{1y} (C_{1y} S_{2y} C_{(1-2)x} - S_{1y} C_{2y}) \right. \\ \left. - \dot{\theta}_{1x} S_{1y} S_{2y} S_{(1-2)x} \right]$$

$$V_{c76} = m_2 l_2^2 \dot{\theta}_{2x} C_{2y} S_{2y}$$

and the other elements in V_c are zeros. The gravity vector \mathbf{G} is provided as follows:

$$\mathbf{G} = [0, 0, 0, (m_1 + m_2) g l_1 S_{1x} C_{1y}, (m_1 + m_2) g l_1 C_{1x} S_{1y} \\ m_2 g l_2 S_{2x} C_{2y}, m_2 g l_2 C_{2x} S_{2y}]^\top.$$

REFERENCES

- [1] X. Shao, L. Xu, and W. Zhang, "Quantized control capable of appointed-time performances for quadrotor attitude tracking: Experimental validation," *IEEE Trans. Ind. Electron.*, vol. 69, no. 5, pp. 5100–5110, May 2022.
- [2] X. Shao, G. Sun, W. Yao, J. Liu, and L. Wu, "Adaptive sliding mode control for quadrotor UAVs with input saturation," *IEEE/ASME Trans. Mechatron.*, vol. 27, no. 3, pp. 1498–1509, Jun. 2022.
- [3] B. Zhao, B. Xian, Y. Zhang, and X. Zhang, "Nonlinear robust adaptive tracking control of a quadrotor UAV via immersion and invariance methodology," *IEEE Trans. Ind. Electron.*, vol. 62, no. 5, pp. 2891–2902, May 2015.
- [4] K. Zhang, Y. Shi, and H. Sheng, "Robust nonlinear model predictive control based visual servoing of quadrotor UAVs," *IEEE/ASME Trans. Mechatron.*, vol. 26, no. 2, pp. 700–708, Apr. 2021.
- [5] X. Wang and W. Wang, "Extended signal-correction observer and application to aircraft navigation," *IEEE Trans. Ind. Electron.*, vol. 67, no. 4, pp. 3149–3156, Apr. 2020.
- [6] B. Liu, W. Ni, R. P. Liu, Q. Zhu, Y. J. Guo, and H. Zhu, "Novel integrated framework of unmanned aerial vehicle and road traffic for energy-efficient delay-sensitive delivery," *IEEE Trans. Intell. Transp. Syst.*, vol. 23, no. 8, pp. 10692–10707, Aug. 2022.
- [7] P. E. I. Pounds, D. R. Bersak, and A. M. Dollar, "Grasping from the air: Hovering capture and load stability," in *Proc. IEEE Int. Conf. Robot. Autom.*, 2011, pp. 2491–2498.
- [8] J. Thomas, G. Loianno, K. Sreenath, and V. Kumar, "Toward image based visual servoing for aerial grasping and perching," in *Proc. IEEE Int. Conf. Robot. Autom.*, 2014, pp. 2113–2118.
- [9] R. Spica, A. Franchi, G. Oriolo, H. H. Blthoff, and P. R. Giordano, "Aerial grasping of a moving target with a quadrotor UAV," in *Proc. IEEE/RSJ Int. Conf. Intell. Robots Syst.*, 2012, pp. 4985–4992.
- [10] S. Kim, H. Seo, S. Choi, and H. J. Kim, "Vision-guided aerial manipulation using a multirotor with a robotic arm," *IEEE/ASME Trans. Mechatron.*, vol. 21, no. 4, pp. 1912–1923, Aug. 2016.
- [11] M. Jafarinassab, S. Siroouspour, and E. Dyer, "Model-based motion control of a robotic manipulator with a flying multirotor base," *IEEE/ASME Trans. Mechatron.*, vol. 24, no. 5, pp. 2328–2340, Oct. 2019.
- [12] S. Kim, S. Choi, and H. J. Kim, "Aerial manipulation using a quadrotor with a two DOF robotic arm," in *Proc. IEEE/RSJ Int. Conf. Intell. Robots Syst.*, 2013, pp. 4990–4995.
- [13] S. Tang, V. West, and V. Kumar, "Aggressive flight with suspended payloads using vision-based control," *IEEE Robot. Autom. Lett.*, vol. 3, no. 2, pp. 1152–1159, Apr. 2018.
- [14] L. Qian and H. H. T. Liu, "Path-following control of a quadrotor UAV with a cable-suspended payload under wind disturbances," *IEEE Trans. Ind. Electron.*, vol. 67, no. 3, pp. 2021–2029, Mar. 2020.
- [15] S. Yang and B. Xian, "Energy-based nonlinear adaptive control design for the quadrotor UAV system with a suspended payload," *IEEE Trans. Ind. Electron.*, vol. 67, no. 3, pp. 2054–2064, Mar. 2020.
- [16] C. A. Avelar and J. M. Valenzuela, "New feedback linearization-based control for arm trajectory tracking of the Furuta pendulum," *IEEE/ASME Trans. Mechatron.*, vol. 21, no. 2, pp. 638–648, Apr. 2016.
- [17] J. M. Valenzuela, C. A. Avelar, S. A. P. Guzmán, and V. Santibáñez, "Adaptive neural network control for the trajectory tracking of the Furuta pendulum," *IEEE Trans. Cybern.*, vol. 46, no. 12, pp. 3439–3452, Dec. 2016.
- [18] X. Wu, K. Xu, M. Lei, and X. He, "Disturbance-compensation-based continuous sliding mode control for overhead cranes with disturbances," *IEEE Trans. Automat. Sci. Eng.*, vol. 17, no. 4, pp. 2182–2189, Oct. 2020.
- [19] Y. Qu and L. Cai, "Nonlinear positioning control for underactuated unmanned surface vehicles in the presence of environmental disturbances," *IEEE/ASME Trans. Mechatron.*, vol. 27, no. 6, pp. 5381–5391, Dec. 2022.
- [20] M. M. Nicotra, E. Garone, R. Naldi, and L. Marconi, "Nested saturation control of an UAV carrying a suspended load," in *Proc. Amer. Control Conf.*, 2014, pp. 3585–3590.
- [21] S. Dai, T. Lee, and D. S. Bernstein, "Adaptive control of a quadrotor UAV transporting a cable-suspended load with unknown mass," in *Proc. 53rd IEEE Conf. Decis. Control*, 2014, pp. 6149–6154.
- [22] F. A. Goodarzi, D. Lee, and T. Lee, "Geometric control of a quadrotor UAV transporting a payload connected via flexible cable," *Int. J. Control. Autom. Syst.*, vol. 13, no. 6, pp. 1486–1498, 2015.
- [23] X. Liang, Y. Fang, N. Sun, and H. Lin, "Nonlinear hierarchical control for unmanned quadrotor transportation systems," *IEEE Trans. Ind. Electron.*, vol. 65, no. 4, pp. 3395–3405, Apr. 2018.
- [24] G. Yu, D. Cabecinhas, R. Cunha, and C. Silvestre, "Nonlinear backstepping control of a quadrotor-slung load system," *IEEE/ASME Trans. Mechatron.*, vol. 24, no. 5, pp. 2304–2315, Oct. 2019.
- [25] P. K. Muthusamy, M. Garratt, H. Pota, and R. Muthusamy, "Real-time adaptive intelligent control system for quadcopter unmanned aerial vehicles with payload uncertainties," *IEEE Trans. Ind. Electron.*, vol. 69, no. 2, pp. 1641–1653, Feb. 2022.
- [26] G. Yu, D. Cabecinhas, R. Cunha, and C. Silvestre, "Aggressive maneuvers for a quadrotor-slung-load system through fast trajectory generation and tracking," *Auton. Robots*, vol. 46, no. 4, pp. 499–513, 2022.
- [27] A. Akhtar, S. Saleem, and J. Shan, "Path following of a quadrotor with a cable-suspended payload," *IEEE Trans. Ind. Electron.*, vol. 70, no. 2, pp. 1646–1654, Feb. 2023.
- [28] X. Liang, P. Zhang, Y. Fang, H. Lin, and W. He, "Nonlinear control for aerial transportation systems with double-pendulum swing effects," *IEEE Trans. Ind. Electron.*, vol. 68, no. 7, pp. 6020–6030, Jul. 2021.
- [29] R. Ortega and M. W. Spong, "Adaptive motion control of rigid robots: A tutorial," in *Proc. IEEE 27th Conf. Decis. Control*, 1988, pp. 1575–1584.
- [30] N. Sun, Y. Wu, H. Chen, and Y. Fang, "An energy-optimal solution for transportation control of cranes with double pendulum dynamics: Design and experiments," *Mech. Syst. Signal Process.*, vol. 102, pp. 87–101, 2018.
- [31] N. Sun, Y. Wu, X. Liang, and Y. Fang, "Nonlinear stable transportation control for double-pendulum shipboard cranes with ship-motion-induced disturbances," *IEEE Trans. Ind. Electron.*, vol. 66, no. 12, pp. 9467–9479, Dec. 2019.
- [32] K. Sreenath, T. Lee, and V. Kumar, "Geometric control and differential flatness of a quadrotor UAV with a cable-suspended load," in *Proc. 52nd IEEE Conf. Decis. Control*, 2013, pp. 2269–2274.
- [33] K. Sreenath, N. Michael, and V. Kumar, "Trajectory generation and control of a quadrotor with a cable-suspended load - A differentially-flat hybrid system," in *Proc. IEEE Int. Conf. Robot. Automat.*, 2013, pp. 4888–4895.
- [34] H. K. Khalil, *Nonlinear Systems*, 3rd ed. Englewood Cliffs, NJ, USA: Prentice-Hall, 2002.
- [35] J. J. E. Slotine and W. Li, *Applied Nonlinear Control*, Englewood Cliffs, NJ, USA: Prentice-Hall, 1991.



Xin Cai received the B.S. degree in automation from Nankai University, Tianjin, China, in 2022, where she is currently working toward the Ph.D. degree in control science and engineering with the Institute of Robotics and Automatic Information System.

Her research interests include nonlinear control of the unmanned aerial vehicles and aerial manipulation systems.



Hai Yu (Graduate Student Member, IEEE) received the B.S. degree in automation from Jilin University, Changchun, China, in 2020. He is currently working toward the Ph.D. degree in control science and engineering with the Institute of Robotics and Automatic Information System, Nankai University, Tianjin, China.

His research focuses on the nonlinear control of the unmanned aerial vehicles.



Wei He received the B.S. degree in intelligent science and technology from Nankai University, Tianjin, China, in 2019, where he is currently working toward the Ph.D. degree in control science and engineering with the Institute of Robotics and Automatic Information System.

His research interests include motion planning, state estimation, and intelligent control of robots, especially unmanned aerial vehicles and aerial manipulation systems.



Jianda Han (Member, IEEE) received the Ph.D. degree in mechatronic engineering from the Harbin Institute of Technology, Harbin, China, in 1998.

From 1998 to 2003, he was a Visiting Scientist with the City University of Hong Kong, Hong Kong, Michigan State University, East Lansing, MI, USA, and Cornell University, Ithaca, NY, USA. He is currently a Professor with the Institute of Robotics and Automatic Information System, Nankai University, Tianjin, China. His research interests include nonlinear estimation and control, robotics, and mechatronics systems.



Xiao Liang (Member, IEEE) received the B.S. degree in intelligence science and technology from the Hebei University of Technology, Tianjin, China, in 2013, and the Ph.D. degree in control theory and control engineering from Nankai University, Tianjin, in 2018.

He is currently an Associate Professor with the Institute of Robotics and Automatic Information System, Nankai University. His research interests include motion planning and nonlinear control of unmanned aerial vehicle systems.



Yongchun Fang (Senior Member, IEEE) received the B.S. and M.S. degrees in control theory and applications from Zhejiang University, Hangzhou, China, in 1996 and 1999, respectively, and the Ph.D. degree in electrical engineering from Clemson University, Clemson, SC, USA, in 2002.

From 2002 to 2003, he was a Post-Doctoral Fellow with the Sibley School of Mechanical and Aerospace Engineering, Cornell University, Ithaca, NY, USA. He is currently a Professor with the Institute of Robotics and Automatic Information System, Nankai University, Tianjin, China. His research interests include nonlinear control, visual servoing, control of underactuated systems, and atomic force microscopy-based nanosystems.

Dr. Fang was the recipient of the National Science Fund for Distinguished Young Scholars of China. He was an Associate Editor for the *ASME Journal of Dynamic Systems, Measurement, and Control*.